# The water vapor foreign-continuum in the 1.6 $\mu$m window by CRDS at room temperature

Didier Mondelain, S. Vasilchenko, S. Kassi, A. Campargue

# The water vapor foreign-continuum in the 1.6 µm window by CRDS at room temperature

D. Mondelain[1*], S. Vasilchenko[1,2], S. Kassi[1], A. Campargue[1],

[1] Univ. Grenoble Alpes, CNRS, LIPhy, 38000 Grenoble, France
[2] Laboratory of Molecular Spectroscopy, V.E. Zuev Institute of Atmospheric Optics, SB, Russian Academy of Science, 1 Akademician Zuev square, 634021 Tomsk, Russia

*Corresponding author: Didier Mondelain (didier. mondelain@univ-grenoble-alpes.fr)

**Key words**

Water vapor; foreign-continuum; MT_CKD model; CRDS; transparency window; atmosphere

## Abstract

Water vapour foreign-continuum absorption cross-sections, $C_F$, are measured for the first time at room temperature in the 1.6 µm transparency window, of importance for atmospheric applications. The measurements are performed by cavity ring down spectroscopy (CRDS) at 15 selected spectral data points. These data, covering the 5700-6640 $cm^{-1}$ spectral range, are derived from the variation of the absorption signal during pressure ramps of humidified air up to 1 atm with a typical 1% humidity rate. The foreign-continuum absorption was obtained as the excess of the measured loss rate compared to the sum of the loss rate measured with dry air, the local water monomer contribution and the self-continuum absorption. $C_F$ values were derived from the linear dependence of the foreign-continuum absorption with the product of the partial pressures of water vapour and air. The semi-empirical MT_CKD $C_F$ values are found significantly underestimated in the centre of the window. The temperature dependence is discussed using high temperature measurements available in the literature.

## 1. Introduction

Water vapour is known to strongly absorb the infrared radiations in the Earth's atmosphere and thus to play a key role in its radiative budget [1]. In addition to the usual absorption by water rovibrational lines, water vapour is responsible for an absorption slowly varying with wavenumber, the so-called water vapour continuum. Paynter and Ramaswamy studied the impact of this continuum in the atmospheric radiative transfer using their own empirical continuum model (BPS continuum) [2] and the semi-empirical MT_CKD model [3,4]. These models exhibit differences which can be particularly important in the mid- and shortwave IR regions leading to significant changes (up to 1 $Wm^{-2}$) of the atmospheric absorption. It is thus important to produce accurate experimental absorption cross-sections to test and validate these empirical models, in particular in the transparency windows where the relative impact of the continuum is the largest. Since now one decade, large experimental efforts have been performed to complete the pioneer works of Burch [5,6,7], using different techniques: Fourier transform spectroscopy (FTS) [8,9,10,11], cavity enhanced absorption spectroscopy (CEAS) [12,13,14,15,16,17,18,19,20,21], calorimetric interferometry [22,23] and photo-acoustic spectroscopy [24]. This is particularly true for the self-continuum absorption due to the interaction between two water molecules. As a result, the latest version (3.2) of the MT_CKD self-continuum has been recently constrained in the 4.0, 2.1, 1.6 and 1.25 µm windows [25], taking into account most of the CEAS cross-sections of Refs. [16 ,17,18,19,21].

In the case of the foreign-continuum arising from interactions between water molecules and molecular oxygen and nitrogen, scarce experimental data are available [26], in particular at room temperature. This includes in-band continuum measurements in the 3500–4000 $cm^{-1}$ spectral range by direct absorption spectroscopy [7] and between 1300 and 7500 $cm^{-1}$ by FTS [27]. As concerned the transparency windows, cross-sections provided by FTS [28,29,30] in the mid-IR windows and by cavity ring down spectroscopy (CRDS) in the 2.1 µm window [19] have led to a significant increase of the MT_CKD foreign-continuum since the 2.8 version [25]. Note that FTS data were reported by the CAVIAR consortium at high temperature (350-430 K) over the wide 1.1 - 5.0 µm spectral range thus including the 1.6 µm window of present interest [31]. Additional measurements by CRDS are available at 10.6 µm [13], in the 0.94 µm absorption band [32] and, very recently, in the 2.1 µm window by our group [20]. This latter work compared with [31] at high temperature shows a weak positive temperature dependence of the foreign continuum also reported in the infrared in the 296-363 K range [28,29] and in the 260-360 K range near 183 GHz [33].

Note that these experimental investigations, in particular the temperature dependence, may provide insights on the origin of the continuum which can be due to different processes like the far wings of the rovibrational lines, water dimers (in the case of the self-continuum) and collision-induced absorption (CIA) [34,35].

The present work is part of an extensive study that we conduct since several years to better characterize the water vapour continuum absorption in the short-wave and mid-infrared transparency windows [14,15,16,17,18,19,20,21]. The self-continuum including its temperature dependence was investigated by CRDS in these references. Because of the weakness of the signal to be measured, the experiment is particular challenging in the 1.6 µm window. This applies in particular for the foreign-continuum measurements which require relatively large changes in the gas pressure which may affect the optical alignment. In the following part 2, we will present the experimental procedure adopted for the determination of the foreign-continuum cross-sections at room temperature at 15 selected spectral points of the 1.6 µm window. Data acquisition by CRDS and data treatment as well as the error budget will be discussed in part 3 and the resulting data will be compared to experimental data available in the literature and to the MT_CKD model in part 4.

## 2. Experimental

### *2.1 The CRDS setups*

Measurements were performed using two cavity ring down spectrometers. As described in [36], a distributed feedback (DFB) laser diode (either from Eblana Photonics or NEL) is coupled into a high finesse cavity fitted by two mirrors with highly reflective coatings. Our two spectrometers used mirrors optimized for the 1500-1700 nm and the 1730-1840 nm spectral regions The output mirror of the cavity is mounted on a piezoelectric transducer to periodically change the cell length allowing covering one free spectral range (FSR) of the cavity and thus achieving resonance between the laser light and one longitudinal mode of the cavity. After a build-up time necessary to fill the cavity with photons at resonance, the injection of laser light is stopped thanks to an acousto-optic modulator and the purely exponential decay time of photons leaking from the cavity (*i.e.* the ring down (RD) time, $\tau$) is measured with a photodiode. The fitted RD time is directly related to the absorption coefficient of the absorbing gas, $\alpha(\nu)$, through equation (1).

$$\alpha(\upsilon) = \frac{1}{c\tau(\upsilon)} - \frac{1}{c\tau_0(\upsilon)} \quad (1)$$

With $c$ the speed of light, $\nu$ the laser frequency and $\tau_0$ the ring down time with the optical cavity empty or filled with a non-absorbing gas.

To measure the laser frequency, a part of the laser light was directed via a fibre either to an optical interferometer-based wavelength meter (model 621-A IR from Bristol, ±1.5×10$^{-3}$ cm$^{-1}$ accuracy or model WA-1650 from Burleigh, ±1.1×10$^{-3}$ cm$^{-1}$ accuracy) or to a Fizeau wavelength meter (High Finesse WS-U-30 IR, 6.6×10$^{-4}$ cm$^{-1}$ accuracy) depending on the selected data point and on the availability of the instrument.

A 1000 mbar pressure gauge (model 622AB from MKS instruments) was installed on the cavity to continuously measure the total pressure with an accuracy of 0.15% between 100 and 1000 mbar. A temperature sensor (TSic 501 from IST, ±0.1 K accuracy) was fixed on the external wall of the cavity and enveloped by thermal insulation foam to continuously record the temperature.

### *2.2. Data acquisition*

Foreign continuum cross-sections were determined for 15 spectral points between 5700 cm$^{-1}$ and 6640 cm$^{-1}$ (see **Table 1**). Each spectral point corresponds to the frequency of the radiation delivered by a distributed feedback (DFB) laser diode. Some measurements were repeated several times to check the repeatability The spectral points were selected because they are located in spectral intervals mostly free of absorption lines and thus correspond to weak local monomer contribution. The following procedure was adopted to derive the foreign cross-section value at each selected spectral point.

The high finesse cavity was first flushed with dry air (Alphagaz 2 from Air Liquide, purity > 99.9999%) at a total pressure of 700 Torr, regulated with a solenoid valve and a proportional integral software based loop acting on the gas flow. A spectrum, including at least one isolated water line reported in HITRAN2016 [37] with an accuracy between 1% and 2% (called the reference line, hereafter), was recorded to check the low residual water vapour concentration (typically on the order of 100 ppmv). The loss rate, $\frac{1}{c\tau_0(\upsilon)}$, at the laser frequency fixed to one of the selected spectral points was measured during pressure ramp of dry air decreasing from 700 Torr to 350 Torr (**Figure 1**). The typical duration of the pressure ramp was a few minutes.

As mentioned above a major difficulty of the experiment is that the amplitude of the pressure variation required to measure the foreign-continuum induces significant changes in the optical alignment of the CRDS cavity. As illustrated in the dry air recordings of **Fig. 1**, the pressure induced variation of the loss rate is mostly negligible on the edges of the window but, in the centre of the window, reaches values on the order of the additional losses due to water in the humidified air recordings. This would prevent foreign-continuum determination if the observed pressure induced variation were not repeatable. In fact, as illustrated in the superimposed traces of the dry air recordings presented in **Fig. 1**, the pressure effect on the optical alignment was checked to be highly repeatable allowing to use dry air pressure ramps as zero absorption baseline of the humidified air pressure ramps.

After the dry air recording, the cell was evacuated and filled with humidified air up to 700 Torr using a home-made humidifier [20]. Humidified air was flushed until a constant water vapour concentration of typically 1% was achieved (Above this value, the water concentration was not stable enough. In order to check the stability of the water partial pressure, a series of consecutive CRDS spectra, including the reference water line, was recorded. For each spectrum, the concentration was deduced from a fit to the water absorption line using a Voigt profile. Once the water relative concentration in the cell was stabilized within better than 1% (typically after 60 min), the injection of humidified air was stopped and the loss rates were measured at the selected spectral point, during pressure ramp decreasing from 700 to 350 Torr (**Figure 1**). An additional spectrum around the reference line was recorded at 350 Torr to check that the water vapour concentration has remained unchanged during the ramp.

For this type of measurements, the stability of the ramp is essential. This is why we checked carefully both the short-term and long-term stability of our set-up by recording several decreasing and increasing dry air ramps consecutively and comparing dry air ramps recorded at several hours of distance and/or at different days for a given spectral point. We observed a very good repeatability with no detectable changes on the short term scale (**Figure 1**) and changes of $5\times10^{-10}$ cm$^{-1}$ (offset) at maximum on the long term scale (over days) which represents between 2% and 50% of the maximum measured absorption of the foreign-continuum, depending on the considered spectral point. Let us mention that pressure ramps were restricted to the 350 - 700 Torr range as a small hysteresis, probably caused by changes in the mirror alignment, was observed when the cell was fully evacuated. Note that the procedure described here based on pressure ramps at fixed frequency was adopted because it is less time consuming than that applied in reference [20], where spectra of air with different water vapour concentrations were recorded.

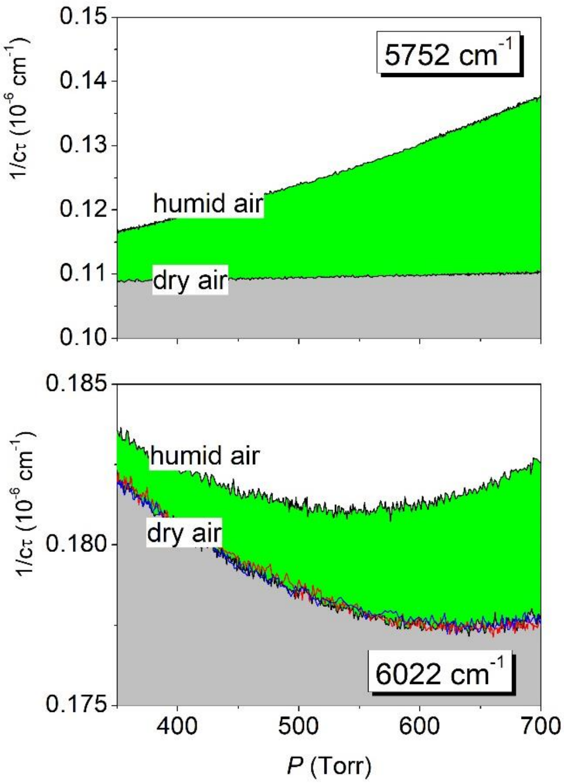


*Figure 1. Variation of the CRDS loss rate for humidified and dry air pressure ramps on the low energy edge (5752 cm$^{-1}$) and near the center (6022 cm$^{-1}$) of the 1.6 µm window. Note the variation of the loss rate of the dry air recordings with pressure due to a change of the mirrors alignment. This variation is checked to be repeatable by the superposed results obtained here for three dry air pressure ramps at 6022 cm$^{-1}$ (lower panel). Note the different amplitude of the losses due to water vapor (green) at 5752 cm$^{-1}$ and 6022 cm$^{-1}$*

## 3. Analysis and resulting $C_F$ cross-sections

### *3.2 Data analysis and $C_F$ cross-sections retrieval*

In a mixture of water vapor in air, the total absorption coefficient can be expressed as the sum of four terms:

$$\alpha_{tot}(\nu,T) = \alpha_{cavity} + \alpha_{WML} + \alpha_{WCS} + \alpha_{WCF}$$

$$= \alpha_{cavity} + \alpha_{WML} + \frac{1}{kT}C_S(\nu,T)P_{H_2O}^2 + \frac{1}{kT}C_F(\nu,T)P_{H_2O}P_{air} \quad (2)$$

where $\alpha_{cavity}$, $\alpha_{WML}$, $\alpha_{WCS}$ and $\alpha_{WCF}$ are the contributions due to the cavity, water vapor "monomer local lines" (WML), water vapor self-continuum (WCS) and foreign-continuum (WCF), respectively. $C_S$ and $C_F$ cross-sections are expressed in cm$^2$molecule$^{-1}$atm$^{-1}$.

From Equation (2), the foreign continuum absorption for a total pressure $P= P_{air}+P_{H_2O}$, is thus obtained by subtracting three contributions from the measured humidified air absorption ($\alpha_{tot}$): the dry air signal ($\alpha_{cavity}$) for the same total pressure, $P$, corresponding to the losses of the cavity in absence of water vapor, the contribution of the air-broadened rovibrational lines, $\alpha_{WML}$, and the water vapor self-continuum absorption at the $P_{H_2O}$ partial pressure. Note that at a total pressure of 700 Torr, losses due to Rayleigh scattering in dry air and in air humidified with 1% water concentration differ by a negligible quantity of $2\times10^{-11}$ $cm^{-1}$ calculated from [38].

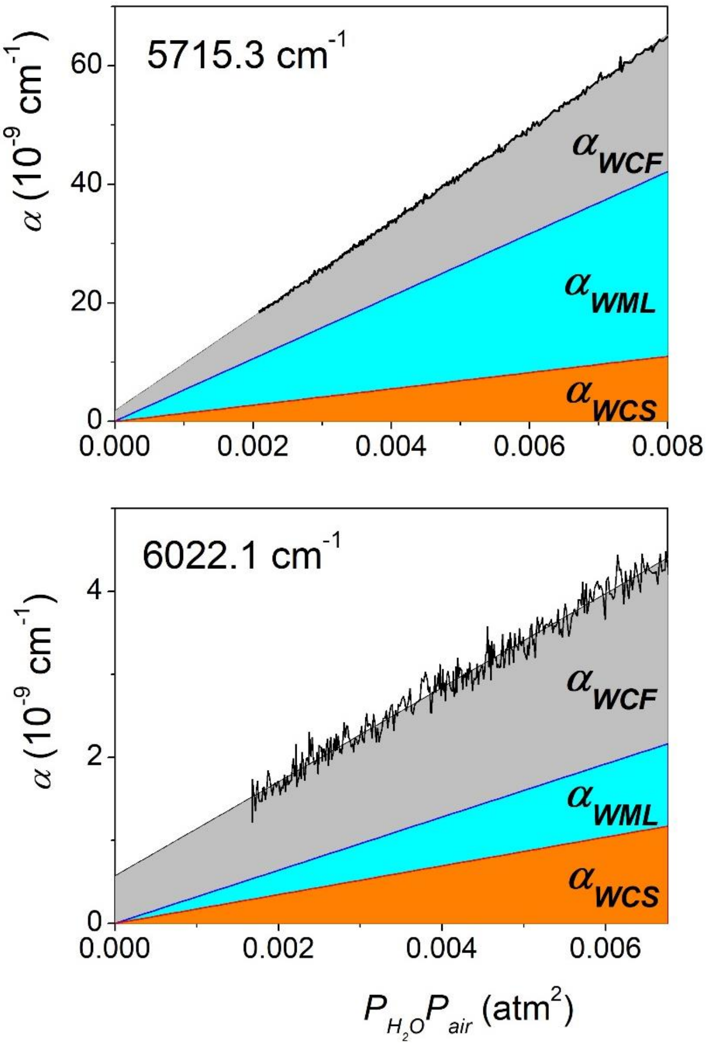


*Figure 2. Humidified air pressure ramp recorded at 5715.30 $cm^{-1}$(left panel) and 6022.06 $cm^{-1}$ (right panel) after subtraction of the dry air ramp (black solid line). The water monomer local contribution ($\alpha_{WML}$), the self- ($\alpha_{WCS}$) and the foreign-continuum contributions ($\alpha_{WCF}$) are also plotted. The water relative concentration, $\boldsymbol{P_{H_2O}/P_{air}}$, on the order of 1% was maintained constant during the pressure ramp.*

After subtraction of the baseline, the quantity $\alpha_{tot} - \alpha_{cavity} = \alpha_{WML} + \alpha_{WCS} + \alpha_{WCF}$ shows a linear dependence with $P_{H_2O}P_{air}$ as illustrated in **Figure 2**. In particular, note the linearity of $\alpha_{tot} - \alpha_{cavity}$ achieved at 6022.1 $cm^{-1}$ confirming that the pressure effects on the mirror alignment, although important (see lower panel of **Figure 1**), is corrected by using the dry air measurements. The lines contribution was simulated at the selected spectral points, for total pressures of 350, 500, 600 and 700 Torr and the $P_{H_2O}$ partial pressure fixed to its measured value (corresponding to about 1% concentration). Simulations were performed using the

HITRAN2016 line list [37], using a Voigt profile and the standard [-25 $cm^{-1}$, +25 $cm^{-1}$] convention cut-off for the line wings [9]. The selected spectral points, $\nu_i$, being located at frequency values far from line centers, the pressure dependence of $\alpha_{WML}$ is proportional to $P_{H_2O}P_{air}$. The pressure dependence of the simulated $\alpha_{WML}$ values were thus fitted with a second order polynomial which was used to subtract the local line contribution over the pressure ramp (**Figure 2**). The self-continuum contribution was calculated using the self-continuum cross-sections from [20]. As the pressure ramps were performed at constant humidity rate ($P_{H_2O}/P_{air}$≈ 1%), $\alpha_{WCS}$ is also proportional to $P_{H_2O}P_{air}$. The relative contributions of the local monomer and of the self- and foreign-continuum, to the total absorption are provided in **Table 1**.

**Figure 3** shows the achieved linear dependence of $\alpha_{WCF}$ *versus* $P_{H_2O}P_{air^r}$ for different selected spectral points. The change of the slope illustrates the frequency dependence of the foreign-continuum cross-sections which were derived from a linear fit (Eq.2). A small positive offset is observed at null pressure. The origin of this offset is not clear. After several tests, we only observed that the slope seems not being affected by a change of the offset value. No offset of this sort was observed in our previous measurements in the 2.3 µm window [20].

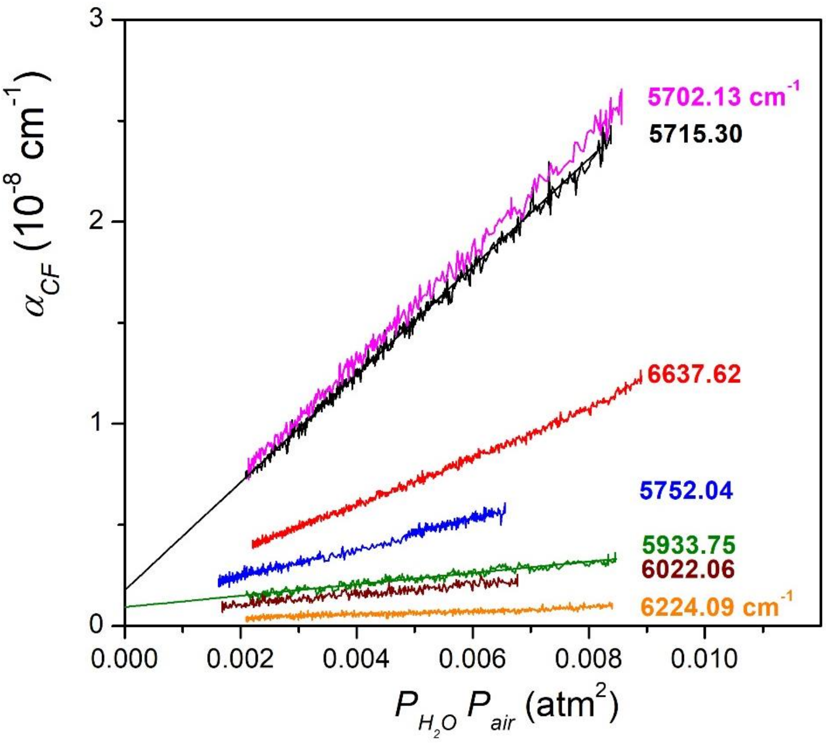


*Figure 3. Absorption coefficient of the foreign-continuum for pressure ramps obtained for different selected spectral points. Two linear fit are also added to show the small observed offsets.*

The $C_F$ values derived from the procedure described above are listed in **Table 1** and presented in **Figure 4**. A 5th order polynomial fit of the $C_F$ cross-sections (weighted by their uncertainties) is also shown in **Figure 4** and was used to provide $C_F$ cross-sections every 10 $cm^{-1}$ between 5700 $cm^{-1}$ and 6640 $cm^{-1}$ as Supplementary Material.

*Table 1. Foreign-continuum cross-sections in the 1.6 µm window and their 1σ estimated uncertainties in units of the last digit (in parenthesis). The relative contributions of the "local line monomer", self- and foreign continuum to the total absorption are also given in the three last columns. During the whole period of measurements temperature varied between 296 K and 298.5 K.*

| ν<br>$cm^{-1}$ | $C_F$<br>$cm^2$ $molecule^{-1}$ $atm^{-1}$ | $\alpha_{WML}/\alpha_{tot}$<br>% | $\alpha_{WCS}/\alpha_{tot}$<br>% | $\alpha_{WCF}/\alpha_{tot}$<br>% |
|---|---|---|---|---|
| 5702.13 | $1.12(11)\times10^{-25}$ | 48.5 | 17.9 | 33.6 |
| 5715.30 | $1.07(16)\times10^{-25}$ | 49.1 | 17.3 | 33.6 |
| 5752.04 | $2.88(95)\times10^{-26}$ | 61.0 | 21.3 | 17.7 |
| 5816.60 | $2.60(28)\times10^{-26}$ | 29.4 | 37.3 | 33.3 |
| 5842.20 | $1.61(30)\times10^{-26}$ | 28.8 | 39.7 | 31.5 |
| | $1.90(30)\times10^{-26}$ | | | |
| | $2.20(30)\times10^{-26}$ | | | |
| 5875.20 | $2.42(24)\times10^{-26}$ | 30.5 | 29.3 | 40.2 |
| | $2.33(24)\times10^{-26}$ | | | |
| 5905.72 | $1.33(20)\times10^{-26}$ | 25.5 | 37.1 | 37.4 |
| | $1.76(20)\times10^{-26}$ | | | |
| | $1.53(20)\times10^{-26}$ | | | |
| 5933.75 | $1.03(10)\times10^{-26}$ | 21.3 | 41.5 | 37.2 |
| | $1.21(10)\times10^{-26}$ | | | |
| | $1.14(10)\times10^{-26}$ | | | |
| | $1.17(10)\times10^{-26}$ | | | |
| | $1.17(10)\times10^{-26}$ | | | |
| | $1.15(10)\times10^{-26}$ | | | |
| | $1.18(10)\times10^{-26}$ | | | |
| 6022.06 | $7.4(15)\times10^{-27}$ | 25.9 | 30.6 | 43.5 |
| 6120.45 | $7.0(12)\times10^{-27}$ | 14.6 | 34.0 | 51.4 |
| 6224.09 | $3.5(12)\times10^{-27}$ | 17.9 | 36.6 | 45.5 |
| 6369.00[a] | $<5\times10^{-27}$ | | | |
| 6511.97 | $6.9(65)\times10^{-27}$ | 85.4 | 5.9 | 8.7 |
| 6562.18 | $9.1(40)\times10^{-27}$ | 79.4 | 8.0 | 12.6 |
| 6637.62 | $4.7(14)\times10^{-26}$ | 71.8 | 6.9 | 21.3 |

[a] *Due to the large estimated uncertainty, only an upper limit value can be given at 6369 $cm^{-1}$.*

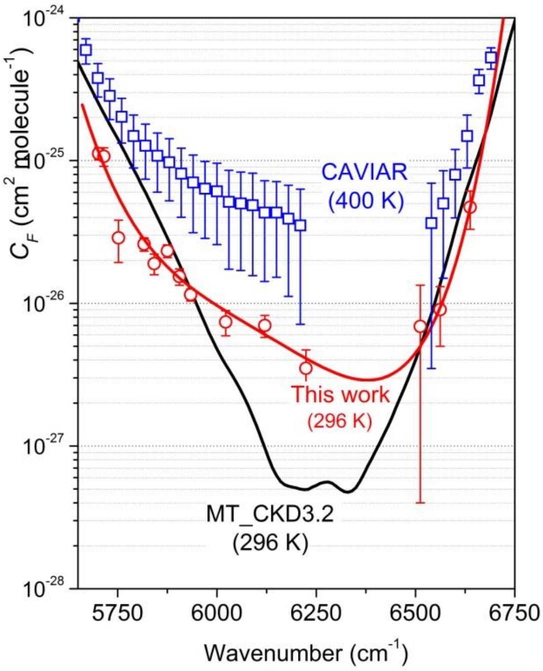


*Figure 4. Overview of the foreign-continuum cross-sections, $C_F$, in the 1.6 µm window obtained in this work and found in the literature. The red solid line corresponds to the fit of our data with a 5$^{th}$ order polynomial. Note that for comparison purposes, the $C_F$ values are density normalized and are given in cm$^2$ molecule$^{-1}$.*

### *3.3 Error budget*

Uncertainties on the derived $C_F$ values have been calculated with the error propagation approach using Eq. 2 and assuming uncorrelated variables. As discussed earlier, the baseline stability was evaluated to be below $5\times10^{-10}$ cm$^{-1}$. Temperature and total pressure are measured with accuracies of 0.1K and 0.15%, respectively. Their contributions are almost negligible. The uncertainties on $C_S$ values used here are reported in [20].

The knowledge on the water vapour partial pressure is the main contributor to the error budget through the monomer contribution which is proportional to $P_{H_2O}$ and the self-continuum contribution proportional to $P^2_{H_2O}$. The partial pressure is derived from the fitted area of well-isolated $H_2O$ lines with intensities reported in HITRAN2016 with uncertainties better than 2% [37]. This value is adopted as the uncertainty on $P_{H_2O}$ considering that the quality figure of the fits, defined as the ratio between peak signal and *rms* fit residuals, of several hundred, limits the error on the fitted area below 1%.

The monomer contribution uncertainties were determined by taking into account the error bars on the line intensities, self-broadening, air-broadening coefficients and water vapour pressure. Four simulations, $\delta_i(\nu)$, were performed, each of them with either, the intensities,

$\gamma_{self}$, $\gamma_{air}$ coefficients or $P_{H_2O}$ values increased by their error bar. The uncertainty on $\alpha_{WML}$ was obtained from: $\delta\alpha_{WML}(\nu) = [\sum_{i=1}^{4} \delta_i(\nu)^2]^{1/2}$.

The uncertainties detailed above are of type-B. To quantify statistical (type-A) uncertainties we recorded consecutively six decreasing pressure ramps of humidified air at the selected spectral point of 5933.75 $cm^{-1}$ chosen because of a limited impact of the uncertainty on $P_{H_2O}$. Between each ramp, the cell was filled again with humidified air from 350 Torr to 700 Torr and two CRDS spectra were recorded to check the stability of the water concentration and determine this concentration. All the ramps were base line corrected using the same dry air ramp recorded just before. Nevertheless, a dry air ramp recorded just after exactly superposed to the ramp used. A relative standard deviation of 2.1% was obtained on the derived $C_F$ values showing the very good short term repeatability. Two months before a $C_F$ value 13% lower than the averaged value on the 6 ramps was measured for the same spectral point with the other CRDS spectrometer used in this work showing that largest statistical uncertainties have to be considered. We also achieved measurements at 5842.24 $cm^{-1}$, 5905.72 $cm^{-1}$ and 6369.00 $cm^{-1}$ done each time at three different days. From these data we extended to each spectral point a statistical uncertainty that we chosen inversely proportional to the ratio between the value of $\alpha_{WCF}$ at 0.08 $atm^2$ (i.e. the maximum of the pressure ramps) and the minimum detectable absorption coefficient $\alpha_{min}$ for the pressure ramp.

Combining the type-A and type-B uncertainties, we obtained the final uncertainties reported in **Table 1** for each spectral point.

## 4 Comparison to literature data

To our knowledge, the only previous determinations of foreign-continuum cross-sections available in the 1.6 µm window have been reported in [31] by the CAVIAR consortium at high temperature. In this work, $C_F$ values were derived from spectra recorded at a single pressure value, with a Fourier transform spectrometer coupled to a White cell providing a 17.7 m optical path length. To increase the absorption continuum signal, the cell was heated between 350 K and 430 K allowing for water vapour partial pressure to be increased up to 266 mbar and 600 mbar, depending on the cell temperature. No temperature dependence of the foreign-continuum could be evidenced in the 350-430 K temperature interval of the FTS measurements. The spectrally smoothed CAVIAR $C_F$ values reported at 400 K [31] are plotted in **Figure 4** with their corresponding error bars ranging between about 25% and 120% on the edges and near the centre of the window, respectively. Overall, the CAVIAR $C_F$ values (density normalized) at 400 K are larger than our cross-sections by factors between ~3 and ~8, on the edges and near the centre of the window, respectively. Such important increase between 296 K and 400 K is significantly larger than the FTS error bars [31] (see **Figure 4**). Nevertheless, the fact that no clear temperature dependence was evidenced between the CAVIAR measurements at 350 K and 430 K questioned the correctness and amplitude of the positive temperature dependence between 296 K and 400 K. Note that in the 2.3 µm window [20], a constant $C_F$ ratio of ~3 was observed over most of the window between the CAVIAR and CRDS cross-sections (density normalized). Again, the significance of this variation close to the 1$\sigma$ error bar of the FTS $C_F$ values, remains to be confirmed.

Finally, let us recall that the foreign-continuum temperature dependence in the windows is by no means similar to that of the self-continuum which exhibits a clear negative temperature dependence (see for example [9,17]).

Foreign-continuum provided by the latest version of the MT_CKD model (MT_CKD3.2) is included in **Figure 4** for comparison purposes. No temperature dependence is provided for the MT_CKD foreign cross-sections. For the low energy edge of the window, the MT_CKD $C_F$ values are significantly larger than our measurements in contrast with the values in the centre of the window which are smaller by a factor of ~9. Nevertheless, near the centre of the window, the foreign continuum is very weak and the experimental uncertainty reaches almost 100%. More accurate measurements are thus required to be conclusive in the very centre of the window, near 6300 cm$^{-1}$.

Finally, let us consider the humidified measurements by calorimetric interferometry reported by Bicknell [22]. In the 2.3 µm window where the continuum is larger, we could calculate the self-contribution to Bicknell's continuum using our determination of the $C_F$ values and obtained a good agreement with our $C_S$ value [20]. In the considered 1.6 µm window, Bicknell reported a total (self+foreign) continuum absorption coefficient of 3.2×10$^{-8}$ cm$^{-1}$ at 6150 cm$^{-1}$ for a mixture of 18.75 Torr of $H_2O$ in $N_2$ with a total pressure of 760 Torr (see [10] for details). For the same experimental conditions, we calculate an absorption coefficient of ~1×10$^{-8}$ cm$^{-1}$ when using our present $C_F$ determination of 5.4(9)×10$^{-27}$ cm$^2$ molec$^{-1}$ atm$^{-1}$ and a $C_S$ value of 4.9(7)×10$^{-25}$ cm$^2$ molec$^{-1}$ atm$^{-1}$ from Ref. [20]. This difference by a factor of 3 is outside the combined error bars and difficult to interpret on the basis of the scarce experimental information provided in Ref.[22] (see [39] for discussion). Note that our $C_F$ determinations rely on careful study of the pressure dependence of the continuum signal while Bicknell's measurements were performed at a single pressure [22].

## 5. Conclusion

Water vapor foreign-continuum cross-sections have been obtained at room temperature in the 1.6 µm window. The corresponding small cross-sections were derived from CRDS measurements during pressure ramps recorded at fixed spectral points between 5700 $cm^{-1}$ and 6640 $cm^{-1}$. Fifteen spectral points were selected to sample the window at frequencies corresponding to small contribution of the water monomer lines. The CAVIAR measurements at high temperature in the same window are larger in amplitude but show a similar wavelength dependence.

The foreign-continuum absorption is very weak at room temperature, in particular, in the very centre of the window. For instance, the absorption coefficient to be measured is on the order of $10^{-9}$ $cm^{-1}$ for 1 atm of humidified air with 1 % of water vapor (≈ 7 Torr). Measurements in this central region were made possible thanks to the very good repeatability of the loss rates of our CRDS set up. Although the dry air CRDS loss rates were found to be sensitive to the pressure variation during the pressure ramp, their dependence was found highly repeatable allowing us to use dry air recordings as baseline of the humidified air recordings.

Two factors could help to decrease the $C_F$ relative uncertainties which range between 10% and 100%. Firstly, our home-made humidifier provides humidified air with stable water vapor relative concentration limited to 1% at most, corresponding to a relative humidity of 33% at 296 K. The increase by a factor of two of the water vapor partial pressure could help to decrease the relative uncertainties. Secondly, the uncertainty on the water vapor partial pressure (or concentration) is the main contributor to the final uncertainties through the self-continuum and the water monomer subtracted contributions. At the moment, a 2% uncertainty is achieved on the knowledge of the water concentration in the used humidified air, mainly due to the uncertainty on the intensity reported in HITRAN2016 for the water reference line used to derive the water partial pressure. Alternative techniques as dew point mirror hygrometers are considered to improve the determination of the water vapor partial pressure by at least a factor of two and thus the accuracy of the reported $C_F$ values, in particular near the centre of the window.

**Acknowledgments**

This project is supported by the Labex OSUG@2020 (ANR10 LABX56) and the LEFE-ChAt program from CNRS-INSU.

## References


[1] Cubasch U, Wuebbles D, Chen D, Facchini MC, Frame D, Mahowald N, Winther J-G, 2013: Introduction. In: Climate Change 2013: The Physical Science Basis. Contribution of Working Group I to the Fifth Assessment Report of the Intergovernmental Panel on Climate Change [Stocker, T.F., D. Qin, G.-K. Plattner, M. Tignor, S.K. Allen, J. Boschung, A. Nauels, Y. Xia, V. Bex and P.M. Midgley (eds.)]. Cambridge University Press, Cambridge, United Kingdom and New York, NY, USA.

[2] Paynter D and Ramaswamy V, Variations in water vapor continuum radiative transfer with atmospheric conditions. J Geophys Res 2012;117:D16310. doi:10.1029/2012JD017504

[3] Clough SA, Kneizys FX, Davies RW. Line shape and the water vapor continuum. Atm Res 1989;23:229-241. doi:10.1016/0169-8095(89)90020-3

[4] Mlawer EJ, Payne VH, Moncet J, Delamere JS, Alvarado MJ, Tobin DC. Development and recent evaluation of the MT_CKD model of continuum absorption. Phil Trans R Soc A 2012;370:2520–2556. doi:10.1098/rsta.2011.0295

[5] Burch DE. Continuum absorption by $H_2O$. Report AFGL-TR-81-0300, Air Force Geophys. Laboratory, Hanscom AFB, MA, 1982.

[6] Burch DE, Alt RL. Continuum absorption by $H_2O$ in the 700 – 1200 $cm^{-1}$ and 2400 – 2800 $cm^{-1}$ windows. Report AFGL-TR-84-0128, Air Force Geophys. Laboratory, Hanscom AFB, MA, 1984.

[7] Burch DE. Absorption by $H_2O$ in narrow windows between 3000 and 4200 $cm^{-1}$. Report AFGL-TR-85-0036, Air Force Geophys. Laboratory, Hanscom AFB, MA, 1985.

[8] Paynter DJ, Ptashnik IV, Shine KP, Smith KM, McPheat R, Williams RG. Laboratory measurements of the water vapor continuum in the 1200–8000 $cm^{-1}$ region between 293 K and 351 K. J Geophys Res 2009;114:D21301. doi:10.1029/2008JD011355

[9] Ptashnik IV, McPheat RA, Shine KP, Smith KM, Williams RG. Water vapor self-continuum absorption in near-infrared windows derived from laboratory measurements. J Geophys Res 2011;116: D16305. doi:10.1029/2011JD015603

[10] Ptashnik IV, Petrova TM, Ponomarev YN, Shine KP, Solodov AA, Solodov AM. Near-infrared water vapour self-continuum at close to room temperature. J Quant Spectrosc Radiat Transfer 2013;120:23–35. doi:10.1016/j.jqsrt.2013.02.016

[11] Ptashnik IV, Petrova TM, Ponomarev YN, Solodov AA, Solodov AM. Water vapor continuum absorption in near-IR atmospheric windows. Atmos Oceanic Opt 2015;28:115–120. doi:10.1134/S102485601502009

[12] Cormier JG, Ciurylo R, Drummond JR. Cavity ringdown spectroscopy measurements of the infrared water vapor continuum. J Chem Phys 2002;116:1030–1034. doi:10.1063/1.1425825

[13] Cormier JG, Hodges JT, Drummond JR. Infrared water vapor continuum absorption at atmospheric temperatures. J Chem Phys 2005;122:114309. doi: 10.1063/1.1862623

[14] Mondelain D, Aradj A, Kassi S, Campargue A. The water vapour self-continuum by CRDS at room temperature in the 1.6 μm transparency window. J Quant Spectrosc Radiat Transfer 2013;130:381–91. doi: 10.1016/j.jqsrt.2013.07.006 .

[15] Mondelain D, Manigand S, Manigand S, Kassi S, Campargue A. Temperature de- pendence of the water vapor self-continuum by cavity ring-down spectroscopy in the 1.6 μm transparency window. J Geophys Res Atmos 2014;119(9):2169–8996. doi: 10.1002/2013JD021319 .

[16] Campargue A, Kassi S, Mondelain D, Vasilchenko S, Romanini D. Accurate laboratory determination of the near infrared water vapor self-continuum: A test of the MT_CKD model. J Geophys Res Atmos 2016;121:13,180 – 13,203. doi:10.1002/2016JD025531

[17] Richard L, Vasilchenko S, Mondelain D, Ventrillard I, Romanini D, Campargue A. Water vapor self-continuum absorption measurements in the 4.0 and 2.1 μm transparency windows. J Quant Spectrosc Radiat Transf 2017;201:171–179. doi: 10.1016/j.jqsrt.2017.06.037

[18] Lechevallier L, Vasilchenko S, Grilli R, Mondelain D, Romanini D, Campargue A. The water vapour self-continuum absorption in the infrared atmospheric windows: new laser measurements near 3.3 and 2.0 μm. Atmos Meas Tech 2018;11:2159–2171. doi:10.5194/amt-11-2159-2018

[19] Mondelain D, Vasilchenko S, Ĉermák P, Kassi S, Campargue A. The self- and foreign-absorption continua of water vapor by cavity ring-down spectroscopy near 2.35 μm. Phys Chem Chem Phys 2015;17:17,762–17,770. doi: 10.1039/c5cp01238d

[20] Vasilchenko S, Campargue A, Kassi S, Mondelain D, The water vapour self- and foreign-continua in the 1.6 μm and 2.3 μm windows by CRDS at room temperature. J Quant Spectrosc Radiat Transfer 2019;227:230–238. doi: 10.1016/j.jqsrt.2019.02.01
[21] Ventrillard I, Romanini D, Mondelain D, Campargue A. Accurate measurements and temperature dependence of the water vapor self-continuum absorption in the 2.1 μm atmospheric window. J Chem Phys 2015;143:134304. doi: 10.1063/1.4931811]
[22] Bicknell WE, Cecca SD, Griffin MK. Search for low-absorption regions in the 1.6- and 2.1-μm atmospheric windows. J Directed Energy 2006;2:151–61.
[23] Fulghum SF, Tilleman MM. Interferometric calorimeter for the measurement of water-vapor absorption. J Opt Soc Am B – Opt Phys 1991;8:2401–2413. Doi:10.1364/josab.8.002401.
[24] Kapitanov VA, Osipov KY, Ptashnik IV. Photoacoustic measurements of the water vapor continuum absorption in the 1.6 μm window. Optika Atmosfery i Okeana 2018;31:995–1000 [in Russian].
[25] http://rtweb.aer.com/continuum_description.html
[26] Hartmann J-M,Tran H, Armante R, Boulet C, Campargue A, Forget F, Gianfrani L, Gordon I, Guerlet S, Gustafsson M, Hodges JT, Kassi S, Lisak D, Thibault F, Toon GC. Recent advances in collisional effects on spectra of molecular gases and their practical consequences, J Quant Spectrosc Radiat Transfer 2018;213:178–227. doi: 10.1016/j.jqsrt.2018.03.016
[27] Paynter D J, Ptashnik I V, Shine K P, Smith K M, McPheat R, Williams R G 2009 Laboratory measurements of the water vapour continuum in the 1200–8000 $cm^{-1}$ region between 293K and 351 K. J Geophys Res 114, D21301. doi:10.1029/2008JD011355
[28] Baranov YI. The continuum absorption in $H_2O+N_2$ mixtures in the 2000–3250 $cm^{-1}$ spectral region at temperatures from 326 to 363 K. J Quant Spectrosc Radiat Transfer 2011;112:2281–2286. doi:10.1016/j.jqsrt.2011.06.005
[29] Baranov YI, Buryak IA, Lokshtanov SE, Lukyanchenko VA, Vigasin AA. $H_2O-N_2$ collision-induced absorption band intensity in the region of the $N_2$ fundamental: ab initio investigation of its temperature dependence and comparison with laboratory data. Phil Trans R Soc A 2012;370:2691–2709. doi: 10.1098/rsta.2011.0189.
[30] Baranov YI and LaffertyWJ. The water vapour self- and water-nitrogen continuum absorption in the 1000 and 2500 $cm^{-1}$ atmospheric windows. Phil Trans R Soc A 2012;370:2578–2589. doi: 10.1098/rsta.2011.0234
[31] Ptashnik IV, McPheat RA, Shine KP, Smith KM, Williams RG. Water vapour foreign-continuum absorption in near-infrared windows from laboratory measurements. Phil Trans R Soc A 2012;370: 2557–2577. doi:10.1098/rsta.2011.0218
[32] Reichert L, Andrés Hernández MD, Burrows JP, Tikhomirov AB, Firsov KM, Ptashnik IV. First CRDS-measurements of water vapour continuum in the 940 nm absorption band. J Quant Spectrosc Radiat Transf 2007;105:303–11. doi:10.1016/j.jqsrt.2006.10.010
[33] Brogniez H, English S, Mahfouf JF, Behrendt A, Berg W, Boukabara S, Buehler SA, Chambon P, Gambacorta A, Geer A, Ingram W, Kursinski ER, Matricardi M, Odintsova TA, Payne VH, Thorne PW, Tretyakov MY, Wang J. A review of sources of systematic errors and uncertainties in observations and simulations at 183 GHz. Atmos Meas Tech 2016;9:2207–2221. doi:10.5194/amt-9-2207-2016
[34] Serov EA, Odintsova TA, Tretyakov MY, Semenov ME. On the origin of the water vapour continuum absorption within rotational and fundamental vibrational bands. J Quant Spectrosc Radiat Transfer 2017;193:1–12. doi: 10.1016/j.jqsrt.2017.02.011
[35] Shine KP, Ptashnik IV, Rädel G. The Water Vapour Continuum: Brief History and Recent Developments, Surv Geophys 2012;33:535–555. doi:10.1007/s10712-011-9170-y
[36] Kassi S, Campargue A. Cavity ring down spectroscopy with $5\times10^{-13}$ $cm^{-1}$ sensitivity. J Chem Phys 2012;137:234201. doi: 10.1063/1.4769974.
[37] Gordon IE, Rothman LS, Hill C, Kochanov RV, Tan Y, Bernath PF, Birk M, Boudon V, Campargue A, Chance KV, Drouin BJ, Flaud JM, Gamache RR, Hodges JT, Jacquemart D, Perevalov, VI, Perrin A, Shine KP, Smith MAH, Tennyson J, Toon GC, Tran H, Tyuterev VG, Barbe A, Császár, AG, Devi VM, Furtenbacher T, Harrison JJ, Hartmann J-M, Jolly A, Johnson TJ, Karman T, Kleiner, I, Kyuberis AA, Loos J, Lyulin OM, Massie ST, Mikhailenko SN, Moazzen-Ahmadi N, Müller HSP,

Naumenko OV, Nikitin AV, Polyansky OL, Rey M, Rotger M, Sharpe SW, Sung K, Starikova E, Tashkun SA, Vander Auwera J, Wagner G, Wilzewski J, Wcisło P, Yu S, Zak EJ. The HITRAN2016 Molecular Spectroscopic Database. J Quant Spectrosc Radiat Transf 2017;203:3-69. doi: 10.1016/j.jqsrt.2017.06.038

[38] Thalman R, Zarzana K, Tolbert MA and Volkamer R. Rayleigh scattering cross-section measurements of nitrogen, argon, oxygen and air. J Quant Spectrosc Radiat Transfer 2014;147:171–177. doi: 10.1016/j.jqsrt.2014.05.030

[39] Shine KP, Campargue A, Mondelain D, McPheat RA, Ptashnik IV, Weidmann D. The water vapour continuum in near-infrared windows – Current understanding and prospects for its inclusion in spectroscopic databases. J Molec Spec 2016;327:193–208. doi: 10.1016/j.jms.2016.04.011